Theory of Electrified Interfaces: A Combined Analysis Using the Density Functional Approach and Bethe Approximation

R. Saradha and M. V. Sangaranarayanan*

Department Of Chemistry, Indian Institute Of Technology, Madras 600 036, India

Received: January 26, 1998; In Final Form: April 6, 1998

A new analysis of the metal/electrolyte interface using jellium model for metal surfaces and Bethe approximation for dipolar interactions is carried out. The total surface energy taking into account the metal−solvent interactions is then solved using a one-parameter family of trial functions for the electronic density profile, and a systematic investigation of the metal−solvent bond length (x_1) and its dependence on electrode charge density (σ^M) is presented. The crucial role played by x_1 in double-layer analysis is also pointed out using the variation of inner layer capacitance with σ^M at the Hg/NaF interface. The model is then used to analyze the effect of temperature, bulk electron density of the metal, and electron−ion coupling terms using Ashcroft pseudopotential on the capacitance−potential plots. The position of the image plane and its variation with electric field, electron density of metals, etc., have also been outlined. The influence of external field on work function changes pertaining to solvent adsorption at electrochemical interfaces is discussed.

I. Introduction

The theoretical description of the electrical double layer at electrode/electrolyte interfaces has always been a major challenge in fundamental electrochemistry. Many in situ spectroscopic techniques[1−3] that have been developed recently provide molecular/microscopic level information regarding the interfacial structure. However, satisfactory reproduction of classical experimental observations[4,5] regarding differential capacitance variation with metal surface, solvent dipoles under varying perturbations such as temperature, applied potential, etc., still remains a formidable task. In view of this, development of microscopic theories for organization of ions and dipoles at metallic surfaces continues to be a frontier area in electrochemistry and surface science. During the past few decades, impressive advances[6−12] have been made in the statistical mechanical theory of solvents in contact with metal surfaces as well as in the quantum mechanical treatment of electronic properties of metals, with the aim of analyzing capacitance−potential behavior and its variants at the metal/electrolyte interface in order to improve the understanding of equilibrium properties of electrochemical interfaces.

These theories of electrical double layer may be classified into primitive and nonprimitive depending upon the description of polarization of solvent molecules and the ion distribution. Primitive models assume that the first monolayer of solvent adjacent to the electrode can be treated as a dielectric slab of varying permittivity, while the remainder of the solution is composed of ions embedded in a dielectric continuum of solvent. In nonprimitive models, distribution functions are calculated for the solvent molecules as well as for ions, with the inclusion of appropriate interaction energies between the species populating the interfacial region.

Although the continuum or nonprimitive models have improved our understanding of double-layer structure, their validity is restricted to near PZC since extension to other surface charge densities becomes tedious. Hence progress in this direction has not been complementary to the efforts involved. On the other hand, monolayer models with discrete orientational states for solvent dipoles adsorbed on the metal surface are still useful in providing new insights as well as hitherto-unknown limitations concerning the interfacial structure. The interaction energy between two polar solvent molecules is usually comparable to the energy of interaction of a solvent dipole at electrode/electrolyte interfaces with the electric field. Thus, a realistic description of the intermolecular electrostatic interactions is of prime importance in the analysis of the interfacial properties. In discrete orientational state models, dipole−dipole interactions are usually calculated from molecular field approximation, which allows only an approximate (sometimes qualitatively inadequate) description since it cannot include short-range correlations. We consider in the present study the efficacy of Bethe approximation for dipolar interactions ascribing two orientational states for solvent dipoles, and this monolayer model is then coupled with the jellium model for the metal. The calculations are also extended with Ashcroft pseudopotential form for the electron ion coupling, within the jellium model. Further, the distance factor in metal−solvent interactions and its variation with surface charge density are analyzed using inner layer differential capacitance−charge curves.

II. Model Analysis

In the present model, the metal is treated using a jellium model[13] with the inclusion of metal−solvent interactions in the total interfacial energy. To take into account the effect of lattice structure, the jellium model has been modified with a lattice of pseudopotentials for electron−ion coupling,[14] and the simplest Ashcroft pseudopotential form has been employed.[15] The above quantum mechanical model is then coupled with a monolayer model of nonpolarizable solvent dipoles oriented in either of the two configurational states ("up" and "down") with equal and opposite dipole moments ($-p$ and $+p$). The dipolar interactions are treated using the Bethe approximation where the interactions within a chosen central cluster are treated exactly. A detailed description of the Bethe approximation pertaining to electrosorbed solvent molecules[16,17] and its coupling with the jellium model is given elsewhere.[18] The total

S1089-5647(98)00885-2 CCC: $15.00
Published on Web 06/18/1998

surface energy at the interface

$$\sigma(n) = \sigma_k + \sigma_{xc} + \sigma_{es} + \sigma_{ps} + \sigma_{cl} + \sigma_R + \sigma_f \qquad (1)$$

is then minimized using a one-parameter family of trial functions for $n(x)$. The explicit expressions for the first three terms are given by Smith.[19] σ_{cl} and σ_R are density profile independent and hence eliminated while minimizing the surface energy.

The trial function employed in our analysis including the external field contribution is[20]

$$n(x) = n - \frac{1}{2}\left(n + \frac{\alpha E_0}{8\pi}\right)e^{\alpha x} \quad \text{for} \quad x < 0$$

$$n(x) = \frac{1}{2}\left(n - \frac{\alpha E_0}{8\pi}\right)e^{-\alpha x} \quad \text{for} \quad x > 0 \qquad (2)$$

where n is the bulk electron density, α is the free parameter that measures the extent of electronic spill over into the exterior, E_0 is the field due to the charge density σ^M on the metal surface ($E_0 = 4\pi\sigma^M$). The pseudopotential contribution within the above family of trial functions is given by

$$\sigma_{ps} = \frac{2\pi n(n + \alpha E_0)}{\alpha^3}\left(1 - \frac{\alpha d\, e^{-\alpha d/2}\cosh(\alpha r_c)}{1 - e^{-\alpha d}}\right) \qquad (3)$$

where d and r_c represent, respectively, the interplanar distance and the pseudopotential core radius. The interaction with the external field σ_f for the present analysis is

$$\sigma_f = \int_{-\infty}^{\infty} [n(x) - n\theta(-x)](E_{dip} + E_0)\, x\, dx$$

$$= \frac{E_0 n}{\alpha^2} + \frac{(1 - e^{-\alpha x_2})E_{dip}}{\alpha^2}\left(\frac{n}{2} - \frac{\alpha E_0}{8\pi}\right) \qquad (4)$$

where x_2 is the sum of metal−solvent bond length (x_1) and the radius of the solvent molecules. E_{dip}, the field due to the solvent dipoles adsorbed on the metal surface, is given by

$$E_{dip} = -\frac{g_{dip}\theta(x)\,\theta(x_2 - x)}{x_2} \qquad (5)$$

where $\Theta(x)$ denotes Heaviside step function and g_{dip} is obtained from the solvent analysis as

$$g_{dip} = -\frac{4\pi N_T p R}{\epsilon} \qquad (6)$$

N_T is the total number of solvent dipoles per unit area, and ϵ is the dielectric constant of the medium. The order parameter, which denotes the extent of orientation of solvent dipoles, is given by[17,18]

$$R = \tanh[k_1 + k_2 z/(z - 1)] \qquad (7)$$

where z is the coordination number of the lattice. $k_1 = pE/kT$ is the contribution due to the external field and takes the form including the jellium field as

$$E = -4\pi \int_{-\infty}^{x_2} [n(x) - n\theta(-x)]dx$$

$$= E_0 + \frac{2\pi n e^{-\alpha x_1}}{\alpha} - \frac{E_0 e^{-\alpha x_1}}{2} \qquad (8)$$

$E_0 = 4\pi\sigma^M/\epsilon$, ϵ being the dielectric constant of the medium, and is equal to unity for metal/vacuum interface. k_2 is given by the following self-consistent equation

$$\exp\left(\frac{2k_2}{z - 1}\right) = \frac{1 + \exp[-2(k_1 + k_2 + \gamma)]}{\exp[-2\gamma] + \exp[-2(k_1 + k_2)]} \qquad (9)$$

where J, the field due to the interaction of a dipole at site "o" with that at site "j", is given by $-p^2/\epsilon z d_s^3$ and d_s is the nearest-neighbor distance. The numerical procedure adopted in the present investigation has been discussed in detail elsewhere.[18]

The total potential drop across the interface is now given by the sum of metal contribution, solvent contribution, metal−solvent interaction terms, and the contribution due to the presence of free charges at the interface as

$$\Delta\Phi_T = \Delta\Phi_M^{(S)} + \Delta\Phi_{dip} + 4\pi x_1\sigma^M - 2\pi d_s\sigma^M - E_0 d_s \qquad (10)$$

where

$$\Delta\Phi_M^{(S)} = 4\pi \int_{-\infty}^{x_2} [n(x) - n\theta(-x)]x\, dx$$

$$= \frac{4\pi n}{\alpha^2} - \frac{2\pi n \exp(-\alpha x_2)}{\alpha^2} + \frac{E_0 \exp(-\alpha x_2)}{2\alpha} \qquad (11)$$

and

$$\Delta\Phi_{dip} = -g_{dip} - \frac{2\pi n x_2 \exp(-\alpha x_1)}{\alpha} + \frac{E_0 x_2 \exp(-\alpha x_1)}{2} \qquad (12)$$

The inner layer capacitance is then obtained by numerically differentiating the potential difference $\Delta\Phi_T$. It may be noted here that when the distance of closest approach of solvent molecules to the metal surface becomes equal to the radius of solvent dipoles, the third and fourth terms of eq 10 vanish and it becomes identical to the expression given for potential drop across the interface by Schmickler.[21] However, in the present study we wish to investigate the variation of x_1 with charge density on the metal surface (σ^M) and its consequences on differential capacitance plots, and hence retained these terms.

Metal−Solvent Bond Length. The distance of closest approach of solvent molecules to the metal surface and its dependence on charge density σ^M are as yet an unsolved problem. In models including the contribution of metal, this issue has been considered by Badiali et al.,[9,22−24] Kornyshev and Vorotyntsev,[25] Halley et al.,[26] Guidelli and Aloisi,[27] and Schmickler and Henderson.[28] The general consensus is that the length of metal−solvent bond varies with the charge density on the metal surface and that it makes an important contribution to the calculated capacitance. The equilibrium distance between jellium and a layer of solvent molecules is obtained from the model calculations incorporating appropriate interaction potentials. Badiali et al. have considered two interaction potentials, viz., (i) a van der Waals pressure attracting the solvent molecules toward the metal, which has been calculated using dispersion force models, and (ii) a strongly repulsive pressure arising from the overlapping of the metal electronic tail with the closed shell of the solvent molecules obtained using a pseudopotential approach. x_1 has then been calculated by minimizing the solvent free energy with respect to x_1 or from the force balance equation, which leads to the introduction of bulk pressure (P) in the calculations. The resulting shape of the $x_1(\sigma^M)$ curve obtained is parabolic with a maximum at moderate negative charge densities. Apart from differences in the estimation of metal−

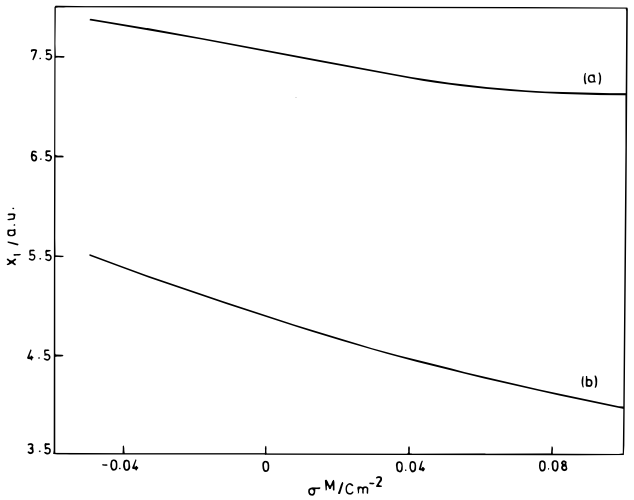

Figure 1. Variation of the distance of closest approach of solvent molecules to the metal surface with charge density on the metal surface: (a) present work and (b) the analysis of Guidelli and Aloisi.[27]

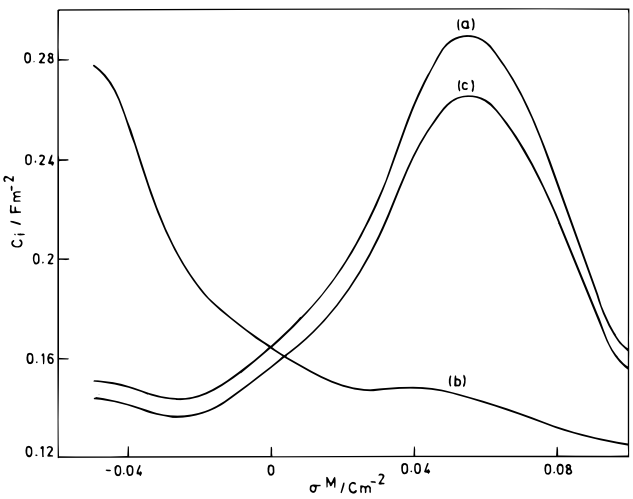

Figure 2. Dependence of inner layer capacitance on charge density at the Hg/NaF interface: (a) without pseudopotential terms, (b) when the metal−solvent bond length is constant, and (c) with averaged pseudopotential contribution to the total surface energy.

solvent interactions, Halley et al. differ from earlier authors in that they minimize the total surface energy with respect to x_1, which leads to the neglect of the effect of P. Hence, the maximum in the $x_1(\sigma^M)$ curve in the calculations of Halley et al. disappears and may occur at more negative charges than observed by Badiali et al. Guidelli and Aloisi[27] have combined the three-dimensional lattice model of TIP4P water molecules with a simple one-parameter jellium model and carried out the estimation of equilibrium distance via an iterative self-consistent procedure based on a balancing of the three pressures, the third one being the electrostatic pressure due to the diffuse layer ions.

Even though extensive numerical calculations have been carried out to obtain x_1, a systematic analysis of double-layer parameters is still lacking owing to the in-built complexity of the problem. In the present study, the variation of x_1 with σ^M is given by the third-degree polynomial as

$$x_1 = a_0 + a_1\sigma_M + a_2\sigma_M^2 + a_3\sigma_M^3 \qquad (13)$$

where the coefficients are $a_0 = 7.56$ br, $a_1 = -7$ br C^{-1} m^2, $a_2 = -2$ br C^{-2} m^4, $a_3 = 300$ br C^{-3} m^6, and br $= 0.529 \times 10^{-10}$ m (Bohr radius). These values have been chosen such that they give satisfactory values for the capacity and the variation of differential capacitance with σ^M for mercury (with capacitance maximum at positive charge densities and decrease in the magnitude of capacitance for higher charges away from PZC). Though the procedure is ad hoc, since our objective is to obtain a qualitative understanding regarding the jellium-based double-layer models, we have restricted ourselves to the same without going into the theoretical basis underlying eq 13. The variation of x_1 with σ^M using eq 13 is shown in Figure 1a, and it resembles the behavior obtained by Guidelli and Aloisi[27] for $\epsilon = 80$, as shown in Figure 1b and by Halley et al.[26] In the present analysis, we have not changed the structure of eq 13 for different metals as well as with different crystal faces of a given metal. The coefficients a_i with $i = 0-3$ are kept constant. Although the methodology is empirical in nature, it (i) reproduces qualitatively the experimental capacitance−potential behavior at the Hg/NaF interface, (ii) yields the correct experimental dependence of inner layer capacitance on bulk electron density of metals, (iii) predicts increase in the effective position of image plane and work function changes due to solvent adsorption with electron density of the metals, and (iv) shows the importance of the parameter x_1 in the model analysis (see below).

III. Results and Discussion

(A) Helmholtz Capacity. The following molecular parameters have been employed for the analysis: The permanent dipole moment $p = 6.13 \times 10^{-30}$ C m, the diameter of the solvent molecules $d_s = 3 \times 10^{-10}$ m, the coordination number of the lattice $z = 6$, the dielectric constant of the medium $\epsilon = 2.3$, the total number of solvent molecules per unit area $N_T = 1 \times 10^{17}$ m^{-2}, the valency of mercury ion $Z_c = 2$, and the pseudopotential core radius of mercury $r_c = 1.12$ au. Figure 2a shows the variation of inner layer capacitance with charge density σ^M on the metal surface for Hg/aqueous electrolyte interface obtained by numerically differentiating eq 10 with respect to σ^M. It can be seen that the capacitance maximum occurs at positive charge densities as observed experimentally.[4] Further, for $\sigma^M \neq 0$ the capacitance decreases as a result of dielectric saturation, which is again consistent with the experimental behavior. We now analyze the effects of various parameters on the calculated inner layer capacitance−potential plots.

(*i*) *Effect of Metal−Solvent Bond Length.* The parameter x_1, which represents the distance of closest approach of solvent molecules to the metal surface, makes an important contribution to the calculated capacitance in the present analysis. This is evidenced by the following observations. The variation of capacitance obtained for different σ^M values maintaining x_1 constant is shown in Figure 2b. It can be noted that the entire shape of the capacitance−charge density plot has now been lost although all other parameters have remained the same. The coefficients in eq 13 also affect the observed behavior of Figure 2a. When a_1 is negative (i.e., if x_1 increases with increasing charge density), the capacitance maximum shifts to slightly negative charge densities, which is not in accordance with the experimental data. Figure 3 represents the effect of decreasing a_0 from 4 to 3.8 Å. There is a marked increase in the capacitance values for the small variation in a_0 with no change in the qualitative behavior. Hence, from the above analysis it is clear that the model reproduces the experimental behavior at the Hg/NaF interface satisfactorily for the set of molecular constants, provided the absolute value of x_1 and its variation with external field are incorporated.

(ii) Effect of Lattice Structure. We investigate here the effect of replacing the uniform background of positive charge by a lattice of pseudopotentials. The metallic ions are assumed to

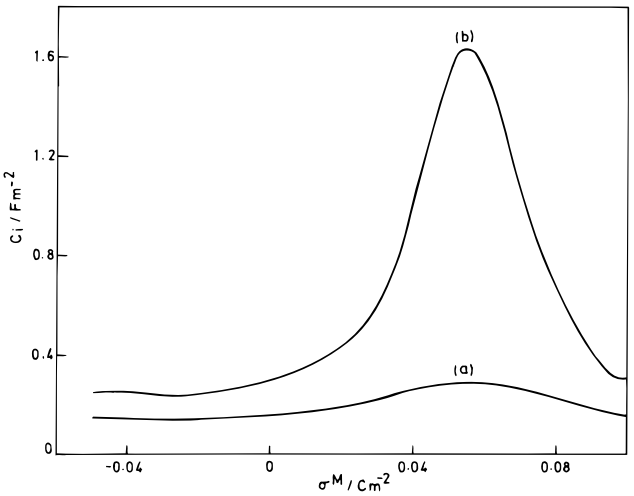

Figure 3. Dependence of capacitance−charge behavior for mercury on the values of metal−solvent bond length (x_1) at PZC (a_0): (a) a_0 = 4 Å (7.56 au) and (b) a_0 = 3.8 Å (7.18 au).

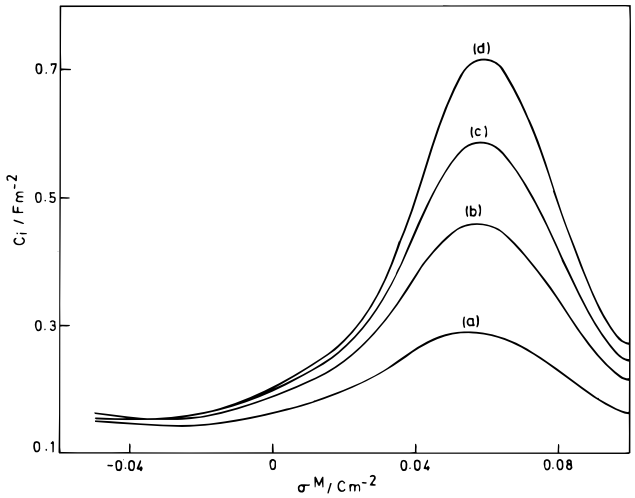

Figure 4. Capacitance−charge behavior as a function of bulk electron density of the metal: (a) n = 0.0127, (b) n = 0.02, (c) n = 0.025, and (d) n = 0.03.

be situated at half of the first lattice plane from the jellium edge. Since our objective is restricted to the study of polycrystalline metal surfaces, the pseudopotential energy has been averaged over various single-crystal planes. The calculations have been carried out for mercury, by assuming fcc crystal structure with three principal planes. The polycrystalline values are then obtained by averaging over their single crystal planes using the expression

$$\sigma_{ps} = \sum_i a_i \sigma_{(ps)i} \tag{14}$$

where a_i is the fraction of the surface occupied by the face i and $\sigma_{(ps)i}$ is the corresponding pseudopotential energy. The relative weights of 111, 100, and 110 faces of the metal are 8/25, 5/25, and 12/25, respectively.[29] Though the above procedure is an approximation, it has been adopted in the present study to show the influence of lattice structure on the double-layer parameters of polycrystalline metals. The same minimization procedure of surface energy using trial functions for the electronic density profile has been followed as before. The values of interplanar spacing (d) employed in the present analysis are taken from the literature. Figure 2c shows the resulting variation of capacitance with charge density, and it is clear that the effect of adding electron−ion coupling terms within the jellium model of the metal is to reduce the capacitance values without altering the qualitative behavior observed in the case of uniform background model. The present analysis neglects the dependence of x_1 on the crystal faces of metal. This aspect becomes important when we investigate solvent structure at different single crystal faces, and since in the present analysis only polycrystalline metals are discussed, the above sophistication is not attempted.

(iii) Effect of Bulk Electron Density and Temperature. We have also analyzed the effect of electron density on the capacitance charge behavior, (Figure 4). With increasing electron density, there is an enhancement in the absolute value of capacitance without any changes in its behavior with respect to surface charge density. For higher values of n there will be more electron spill over from the metal into the solution, which explains the observed increase in the Helmholtz capacity at the interface. Since the variation of electron density is not carried out pertaining to any specific metal, n values have arbitrarily been increased to see the prediction of the present model, and

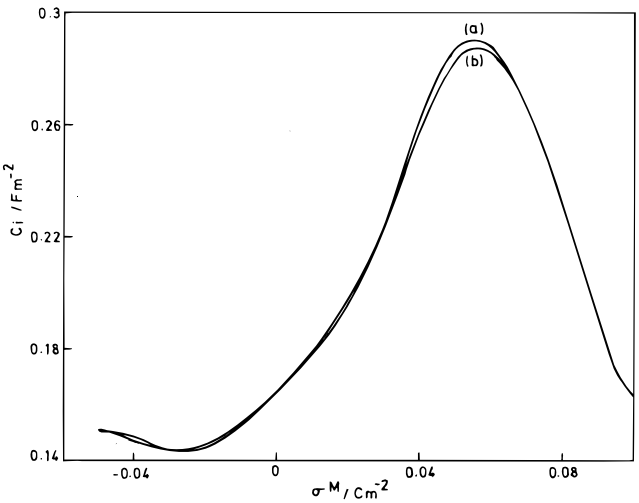

Figure 5. Temperature dependence of inner layer capacitance behavior at the Hg/NaF interface: (a) T = 298 K and (b) T = 378 K.

the distance of closest approach of solvent molecules to the metal surface is maintained at the same value as that used for mercury. The qualitative behavior will be altered if we assume a different parametric dependence of x_1 on σ^M pertaining to various metals. The effect of temperature on the capacitance is shown in Figure 5 since this dependence has generally been used to validate the veracity of solvent models employed in double-layer theories. Figure 5 shows that only minor changes are observed by varying the temperature, and the decrease in capacitance values with temperature as observed experimentally[4] is reproduced. This can be explained as arising from the less orientation of solvent dipoles adsorbed on the surface at higher temperatures.

(B) Image Plane Position. The metal contribution to the capacitance can be related to the effective position of image plane. The electrons on the surface of jellium react to the presence of an external field, unlike a classical conductor. A small test charge situated in front of a jellium surface induces a surface charge of equal magnitude and opposite sign. However, this small excess charge is not located right on the metal surface, the major part lies in front of the jellium edge, and there are oscillations in the induced charge density. As a consequence, the test charge experiences a modified image law, in which the image plane is not situated at the jellium edge,

TABLE 1: Variation of Inner Layer Capacitance and Image Plane Position at PZC for Various Values of Electron Density of the Metal

n (au)	C_i (F m^{-2})	x_{im} (au)	n (au)	C_i (F m^{-2})	x_{im} (au)
0.005	0.111	0.90	0.02	0.188	1.52
0.01	0.149	1.28	0.025	0.197	1.56
0.015	0.174	1.44	0.03	0.203	1.58

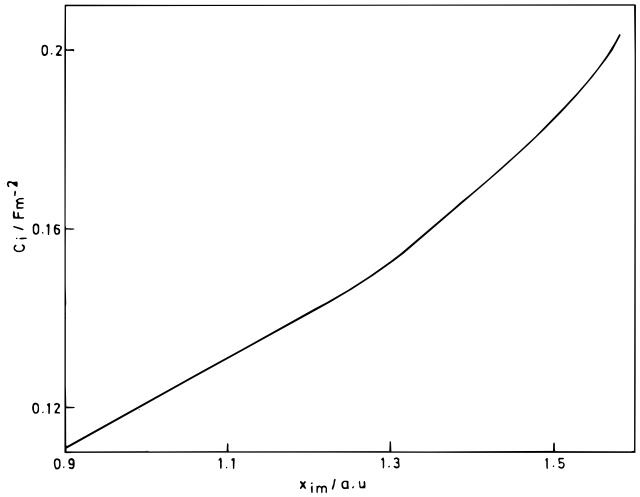

Figure 6. Variation of inner layer capacitance with image plane position at PZC.

where the positive background charge drops to zero, but at a small distance x_{im} in front and is given as[9]

$$x_{im} = -\frac{\partial}{\partial \sigma^M}\int_{-\infty}^{\infty}[n(x) - n\theta(-x)]x\,dx \qquad (15)$$

The image plane position for an uncharged metal surface increases with the electron density, and this is to be expected since a higher electron denisty should entail a greater polarizability. This explains the experimental observation[5,11] of the Helmholtz capacity to increase with the electron density of the metal. The estimation of both C_i and x_{im} at PZC for various values of eletron density of the metal are given in Table 1. Figure 6 shows the dependence of Helmholtz capacity on the effective image plane position calculated for six different values of electron densities at PZC. It shows that there is a direct relationship between inner layer capacitance and image plane position at the electrochemical interfaces. It is also clear that the variation of C_i with n arises owing to the contribution from x_{im} to the total capacitance. Hence, the variation of the parameter x_1 with n makes a smaller contribution to the observed dependence of C_i on n as compared to the effect of x_1 variation with σ^M. The position of the effective image plane depends on the surface charge density. It is higher at negative charge densities where the electrons spill out further than at positive charges, where the electrons are withdrawn toward the bulk. Thus, the response to an external charge is nonlinear, which has important consequences on optical properties such as second-harmonic generation. The variation is shown in Figure 7 for mercury and also for three other hypothetical electronic densities. In the presence of solvent molecules, the effective position (which is obtained from eq 15 with x_2 as the higher limit for the integral) decreases, owing to the interaction of metal electrons with the solvent molecules. This is shown in Figure 8b along with metal/vacuum behavior (Figure 8a). The image plane position obtained by Guidelli and Aloisi[27] using the combined one-parameter jellium model and the three-dimensional lattice model of TIP4P water molecules has also been shown in Figure 8c.

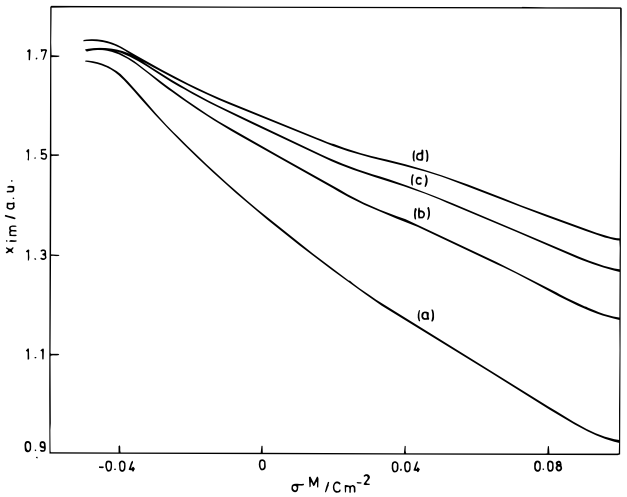

Figure 7. Dependence of image plane position on charge density for different bulk electron density: (a) $n = 0.0127$, (b) $n = 0.02$, (c) $n = 0.025$, and (d) $n = 0.03$.

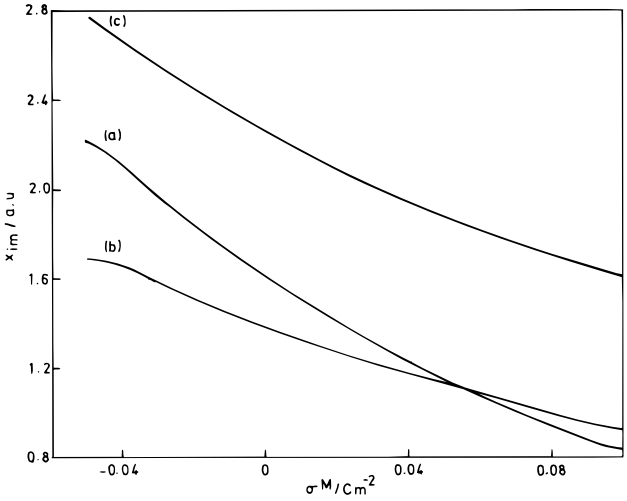

Figure 8. Variation of image plane position with σ^M (a) in the absence and (b) in the presence of adsorbed solvent dipoles for the Hg/NaF interface and (c) from the analysis of Guidelli and Aloisi.[27]

The variation of α, the inverse of which represents the extent of field penetration into the solution, is plotted against various charge densities on the metal surface in Figure 9b. It is clear that this value decreases with increasing the charge density as expected, i.e., there is more field penetration at negative charges whereas the electrons are pulled back into the bulk at positive charge densities. The influence of pseudopotential contribution has also been indicated in Figure 9a. Further, the dependence of extent of field penetration on σ^M pertaining to metal/vacuum interface is also given in Figure 9c. It shows that there is merging of two lines near PZC where adsorption of solvent molecules on the metal surface is weak. Hence the field penetration into solution remains unaltered in this narrow region.

(C) Work Function Changes. The present analysis has also been extended to carry out the variation of work function with charge density on the metal surface. Work function is evaluated using the expression

$$\Phi = \frac{4\pi n}{\alpha^2} - \frac{(3\pi^2 n)^{2/3}}{2} + \left(\frac{3n}{\pi}\right)^{1/3} + \frac{0.056n^{2/3} + 0.0059n^{1/3}}{(0.079 + n^{1/3})^2} \qquad (16)$$

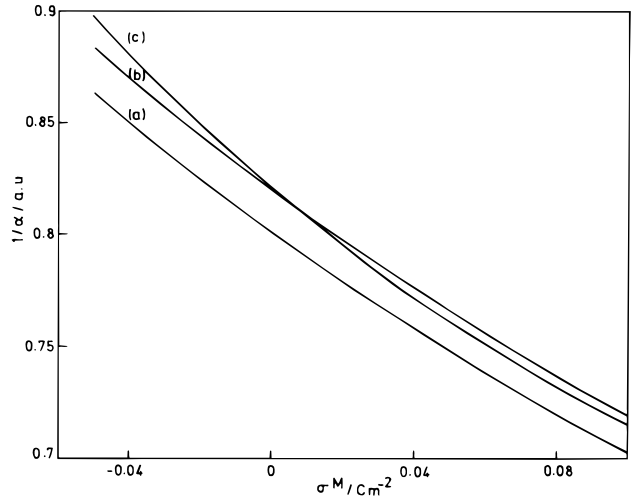

Figure 9. Variation of inverse of the free parameter α with σ^M at the Hg/NaF interface: (a) with pseudopotential contribution to the total energy of the metal, (b) without pseudopotential correction, and (c) for Hg/vacuum interface without pseudopotential contribution.

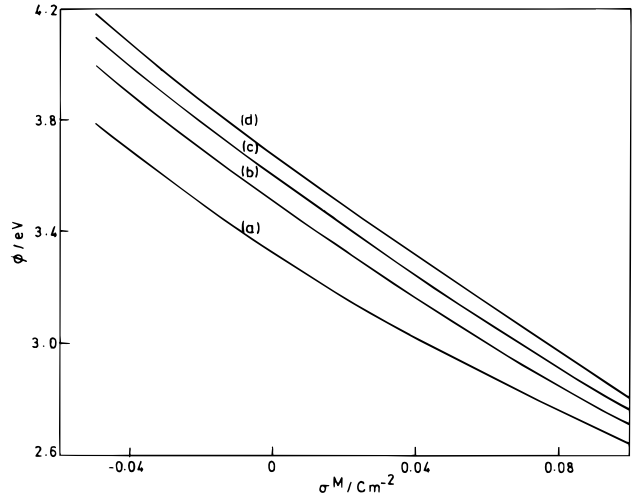

Figure 10. Work function changes with σ^M at electrochemical interfaces: (a) $n = 0.0127$, (b) $n = 0.02$, (c) $n = 0.025$, and (d) $n = 0.03$.

The variation of work function with σ^M for metal/solution interface has been analyzed, and the results are shown in Figure 10. An increase in σ^M leads to a decrease in the work function; i.e., the removal of electrons from the surface of the metal becomes easier when a positive external field operates, and this is to be expected since the positive charge pulls back electrons into the bulk and hence the metal becomes electropositive in nature. Further, when the bulk electron density of the metal is greater than that of Hg, there is a corresponding increase in the work function, which is shown in Figure 10. With increasing electron density, the metals become highly polarized and hence show increase in their work function values; i.e., the metals become electronegative in nature. The inclusion of pseudopotential effects produces only minor changes in the absolute values of work function and hence are not given here.

IV. A Critique of Jellium-Based Double-Layer Models

A comparison with other interfacial models seems necessary at this juncture. In the monolayer model of Schmickler,[21] the discrete solvent molecules are assumed to reach the metal surface until they touch the jellium edge and high values of x_1 and x_2 have been employed. Subsequently, the double layer is treated using a hard sphere ion−dipole model,[28] which has one additional parameter that takes into account the repulsive potential between metal electrons and the solvent molecules and reproduces quantitatively the absolute values of Helmholtz capacity and its variation with electronic density at PZC. To study the capacitance−potential behavior, Schmickler and Henderson[28] have employed a heuristic formula and analyzed the effect of various trial functions for the electronic density profile on capacitance and observed that capacitance maximum occurs at small negative charge values, which is contradictory to the experimental observation at the Hg/aqueous solution interface. Their calculations have also been extended by allowing the variation of the position of hard wall with charge density and observed minor changes in the capacitance−potential behavior. The uniform background model of jellium has been modified by Leiva et al.[30−32] and Schmickler and Henderson[33] to include the lattice effects pertaining to different single-crystal faces of Ag at PZC, and the qualitative experimental trend of inner layer capacitance was reproduced. As a further extension, they have plotted[30] the calculated metal capacitance for the metals of the fourth and fifth column in the periodic table against their experimental inner layer capacitance at PZC. The solvent capacitance was then obtained from the intercept of the plot, which agreed with the estimates predicted by hard sphere models.[28]

Badiali et al.[9,22−24] have assumed that the metal ions are placed on the jellium edge and obtained the distance of closest approach of solvent dipoles to the metal surface through model calculations employing various interaction potentials. Their calculations have showed that the parameter x_1 depends on the charge density on the metal surface as well as upon the crystal faces of the metal. The variation of x_1 makes an important contribution in their analysis. They[9] proceed with a semiempirical approach, in which they obtained first the metal contribution by including the pseudopotential effect and then subtracted the same from the experimental capacitance. The resulting solvent capacitance values were then analyzed for different metal surfaces. They have employed the trial function method for evaluating the electronic density profiles, while Price and Halley[26,34] have investigated a fully self-consistent method for the same. Price and Halley,[26,34] have introduced both one-dimensional and three-dimensional calculations for electronic density profiles and presented the induced charge calculations for jellium slabs in contact with a monolayer of a ordered solvent molecules, which are represented by simple pseudopotentials. The results were used to examine charge distribution at the metallic surface and the influence of the metal−solvent bond length, but the agreement with the experimental behavior with regard to capacitance behavior was still inadequate. They have recently developed[35] a fully self-consistent calculation by combining molecular dynamics and density functional theories so as to obtain preliminary results about the microscopic structure of the electrochemical interfaces.

By combining the three-dimensional model of water molecules with the jellium model of the metal, Guidelli and Aloisi[27] have obtained the differential capacity of the interface with a maximum located at the positive charge densities. Kornyshev et al.[25] have developed a semiphenomenological analysis and used variable distance of closest approach and a rearrangeable free electronic density profile for the analysis of interfacial parameters and showed the importance of the above in the compact layer capacitance curves. The present analysis treats

the solvent molecules as an ordered monolayer that constitutes the inner part of the double layer and agrees with Badiali et al.,[9,22−24] Kornyshev and Vorotyntsev,[25] Price and Halley,[26] and Guidelli and Aloisi[27] in the treatment of distance of closest approach of solvent molecules to the metal surface except that x_1 is evaluated in an empirical manner in the present study. The incorporation of the Bethe approximation for dipolar interactions and coupling the same with the jellium model for metal surfaces carried out here provides scope for further hierarchial developments on solvent dipolar organization using more refined statistical mechanical versions.

V. Summary

Though various models have been developed for double-layer analysis at electrochemical interfaces, none of them has been able to reproduce the quantitative behavior of capacitance−potential plot in a rigorous and self-consistent manner until now. Hence there is a need for further improvements along this line and in the incorporation of novel interaction schemes. The models that provide constancy of the distance of closest approach of solvent molecules to the metal surface seem inadequate. In the present study, the metal is treated using a jellium version within density functional formalism, which is coupled with a monolayer model of solvent molecules employing the Bethe approximation for dipolar interactions. A special emphasis is made on the equilibrium position of solvent molecules with respect to the metal surface and its variation with charge density. The occurrence of capacitance maximum at positive charge densities is correctly predicted. The model explains the influence of bulk electron density and pseudopotential effects on the observed inner layer capacitance and also shows that, with increasing temperature, dipoles become less oriented, and as a result, there is a decrease in the inner layer capacitance. The present calculations also indicate a shift in the effective position of image plane with increasing σ^M and predicts increase in its value with the electron density that is due to the enhanced electronic spill over into the solution. In the presence of solvent molecules, the effective position of the image plane is found to decrease as compared to its value in a vacuum. Further, the present analysis outlines the variation of work function with external field as well as with electronic density for metal/electrolyte interfaces. The analysis can be further extended to obtain a quantitative description of metal−solvent bond length and its variation with external field and with various metals and single-crystal faces. The Bethe approximation employed here can be further improvised with infinite orientational states for solvent molecules and assuming the dipoles to be polarizable. Further investigations employing better trial functions for the electronic density profile seem promising.

References and Notes

(1) Porter, J. D.; Zinn, A. S. *J. Phys. Chem*. **1993**, *97*, 1190.
(2) Toney, M. F.; Howard, J. N.; Richer, J.; Borges, G. L.; Gordon, J. G.; Melroy, O. R.; Wiesler, D. G.; Yee, D.; Sorensen, L. B. *Nature (London)* **1994**, *368*, 444.
(3) Abruna, H. D., Ed. *Electrochemical Interfaces*; VCH: New York, 1991.
(4) Rangarajan, S. K. In *Specialist Periodical Reports, Electrochemistry*; Thirsk, H. R., Ed.; The Chemical Society: London, 1980; Vol. 7.
(5) Parsons, R. *Chem. Rev*. **1990**, *90*, 813.
(6) Schmickler, W. In *Trends in Interfacial Electrochemistry*, Silva, A. F., Ed.; Reidel: Dordrecht, 1986; p 453.
(7) Schmickler, W.; Henderson, D. *Prog. Surf. Sci*. **1986**, *22*, 323. Schmickler, W. In *Structure of Electrified Interfaces*; Lipkowski, J., Ross, P. N., Eds.; VCH Publishers, New York, 1993; p 201.
(8) Kornyshev, A. A. Electrochim. Acta **1989**, *34*, 1829. Kornyshev, A. A. In Condensed Matter Physics Aspects of Electrochemistry; Tosi, M. P., Kornyshev, A. A., Eds.; World Scientific: Singapore, 1991; p 7. Kornyshev, A. A.; Kuznetsov, A. M.; Makov, G.; Vigdorovitch, M. V. *J. Chem. Soc*., Faraday Trans. **1996**, *92*, 3997, 4005.
(9) Badiali, J. P. Electrochim. Acta **1986**, *31*, 149. Badiali, J. P.; Amokrane, S. In *Condensed Matter Physics Aspects of Electrochemistry*, Tosi, M. P., Kornyshev, A. A., Eds.; World Scientific: Singapore, 1991; p 157. Amokrane, S.; Badiali, J. P. in *Modern Aspects of Electrochemistry*, Conway, B. E., White, R. E., Bockris, J. O'M. Eds.; Plenum Press: New York, 1992; Vol. *22*, p 1.
(10) Henderson, D. in *Trends in Interfacial Electrochemistry*; Silva, A. F., Ed. ; Reidel: Dordrecht, 1986.
(11) Schmickler, W. *Chem. Rev*. **1996**, *96*, 3177.
(12) Berard, D. R.; Kinoshita, M.; Cann, N. M.; Patey, G. N. *J. Chem. Phys*. **1997**, *107*, 4719 and references therein.
(13) Lang, N. D.; Kohn, W. *Phys. Rev*. **1970**, *B1*, 4555; **1971**, *B3*, 1215.
(14) Monnier, R.; Perdew, J. P. *Phys. Rev*. **1978**, *B17*, 2595.
(15) Ashcroft, N. W. *Phys. Lett*. **1966**, *23*, 48.
(16) Saradha, R.; Sangaranarayanan, M. V. *J. Chem. Phys*. **1996**, *105*, 4284.
(17) Saradha, R.; Sangaranarayanan, M. V. *J. Colloid Interface Sci*. **1996**, *183*, 610.
(18) Saradha, R.; Sangaranarayanan, M. V. *J. Phys. Chem. B*, in press.
(19) Smith, J. R. *Phys. Rev*. **1969**, *181*, 522.
(20) Partenskii, M.; Smorodinskii, Ya. *Sov. Phys. Solid State, Engl. Transl*. **1974**, *16*, 423.
(21) Schmickler, W. J. *Electroanal. Chem*. **1983**, *150*, 19.
(22) Amokrane, S.; Russier, V.; Badiali, J. P. *Surf. Sci*. **1989**, *217*, 425.
(23) Amokrane, S.; Badiali, J. P. *Electrochim. Acta* **1989**, *34*, 39.
(24) Amokrane, S.; Badiali, J. P. *J. Electroanal. Chem*. **1989**, *150*, 315.
(25) Kornyshev, A. A.; Vorotyntsev, M. A. *J. Electroanal. Chem*. **1984**, *167*, 1.
(26) Halley, J. W.; Price, D. *Phys. Rev*. **1987**, *B35*, 9095; **1988**, *B38*, 9357.
(27) Guidelli, R.; Aloisi, G. In Condensed Matter Physics Aspects of Electrochemistry; Tosi, M. P., Kornyshev, A. A., Eds.; World Scientific: Singapore, 1991; p 139.
(28) Schmickler, W.; Henderson, D. *J. Chem. Phys*. **1984**, *80*, 3381; **1986**, *85*, 1650.
(29) Valette, G.; Hamelin, A. *J. Electroanal. Chem*. **1973**, *45*, 301.
(30) Leiva, E.; Schmickler, W. *J. Electroanal. Chem*. **1986**, *205*, 323.
(31) Leiva, E. *Chem. Phys. Lett*. **1991**, *187*, 143.
(32) Leiva, E.; Schmickler, W. *Surf. Sci*. **1993**, *291*, 226.
(33) Schmickler, W.; Henderson, D. *J. Chem. Phys*. **1985**, *82*, 2825.
(34) Price, D.; Halley, J. W. *J. Electroanal. Chem*. **1983**, *150*, 347. Halley, J. W.; Johnson, B.; Price, D.; Schwalm, M. *Phys. Rev*. **1985**, *B31*, 7695.
(35) Price, D. L.; Halley, J. W. J. Chem. Phys. 1995, **102**, 6603.